The LaGrange case history: inverted pavement system characterisation and preliminary numerical analyses

Douglas D. Cortes & J. Carlos Santamarina

Taylor & Francis
Taylor & Francis Group

The LaGrange case history: inverted pavement system characterisation and preliminary numerical analyses

Douglas D. Cortes[a]* and J. Carlos Santamarina[b]

[a]*Civil Engineering, New Mexico State University, 3035 S. Espina Street, Hernandez Hall, Las Cruces, NM 88003, USA; [b]Civil and Environmental Engineering, Georgia Institute of Technology, 790 Atlantic Drive, Mason Building, Atlanta, GA 30332, USA*

Inverted pavement systems consist of an unbound aggregate base placed between a stiff cement-treated foundation and a thin asphalt cover. Unlike conventional pavements, which rely on stiff bound aggregate layers to bear and spread traffic loads, in an inverted pavement structure, the unbound aggregate inter-layer plays a major role in the mechanical response. A comprehensive characterisation study was conducted during the construction of a full-scale inverted pavement section in LaGrange, GA, USA, with particular emphasis on the unbound aggregate base. New laboratory and *in situ* tests were developed and used to characterise the unbound aggregate non-linear stiffness–stress relationship. Forensic digital image analysis confirmed particle alignment, i.e. inherent anisotropy. Comparison of pre- and post-compaction gradation test results failed to quantify the extent and significance of particle crushing. The information compiled during the field test was used in a complementary numerical study; the results confirm acceptable stress levels within the various layers under standard loads.

Keywords: case history; inverted pavement; unbound aggregate; non-linear behaviour; characterisation; simulations

Introduction

The search for alternative pavement structures seeks improved road performance, energy-efficient pavement solutions and the optimal use of limited natural resources within the framework of economic constraints. Inverted pavement systems have been used as affordable and structurally competent pavement structures in South Africa since the 1950s (Horne *et al.* 1997, Rust *et al.* 1998, Beatty *et al.* 2002). The South African flexible pavement design emphasises the importance of a good foundation, and involves novel construction methods and thorough material selection to achieve dense unbound aggregate layers that exhibit a remarkable ability to support the heaviest traffic loads under both dry and wet conditions (Horne *et al.* 1997). In inverted pavement structures, the cement-treated base provides a suitable foundation, both during compaction and throughout the service life of the unbound aggregate layer (Jooste and Sampson 2005). The South African experience and the body of knowledge accumulating in the USA show that inverted pavements can outperform conventional flexible pavement structures (Ahlvin *et al.* 1971, Barker *et al.* 1973, Grau 1973, Barksdale 1984, Tutumluer and Barksdale 1995, Rasoulian *et al.* 2000, 2001).

The use of inverted pavement structures in the USA has been hindered by the lack of field experiments and related research required to investigate the mechanical response of this pavement structure under local conditions and construction practices. In order to advance the understanding of inverted pavement systems, a full-scale field study was conducted in collaboration with the Georgia Department of Transportation (GDOT). The study documented herein was designed to gather detailed information before, during and after the construction of an inverted pavement test section in LaGrange, GA, USA, in order to gain the critically needed understanding of the internal behaviour and macro-scale performance of this pavement structure through complementary analytical and numerical studies. Detailed information can be found in Cortes (2010).

Project description

The test section constructed in LaGrange is part of an industrial parkway intended to serve the growing car manufacturing industry in southwest Georgia. The inverted pavement test section is a two-lane, 1036 m long stretch of the south LaGrange loop (Figure 1). It was designed to sustain an initial one-way annual average traffic of 7000 vehicles per day, projected to grow to 11,700 by the end of its service life. Truck traffic is estimated at 7% and consists of 3% multi-unit (truck, tractor, semi-trailers and full trailer combination vehicles) and 4% single-unit (two- and three-axle trucks and busses having six tires) trucks.

The test section cuts across residual soils from the Georgia Piedmont geologic formation. Figure 2(a) shows

---

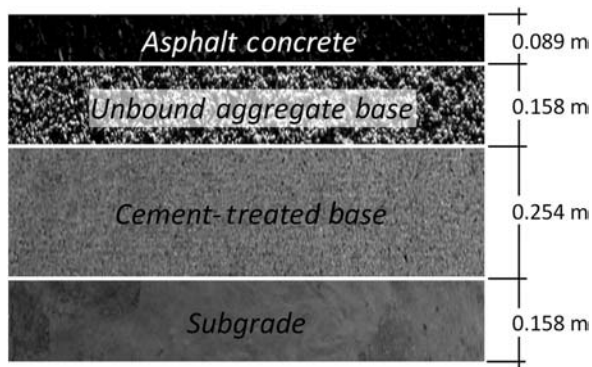*Corresponding author. Email: dcortes@nmsu.edu

Figure 1.   Designed inverted pavement test section.

the original topography and the built longitudinal cross section. Material removed from the cut sections was transported and compacted in the two fill sections. Construction of the subgrade took place from 7 January 2008 to 19 February 2008. Field compaction compliance tests conducted on the subgrade failed to meet the design
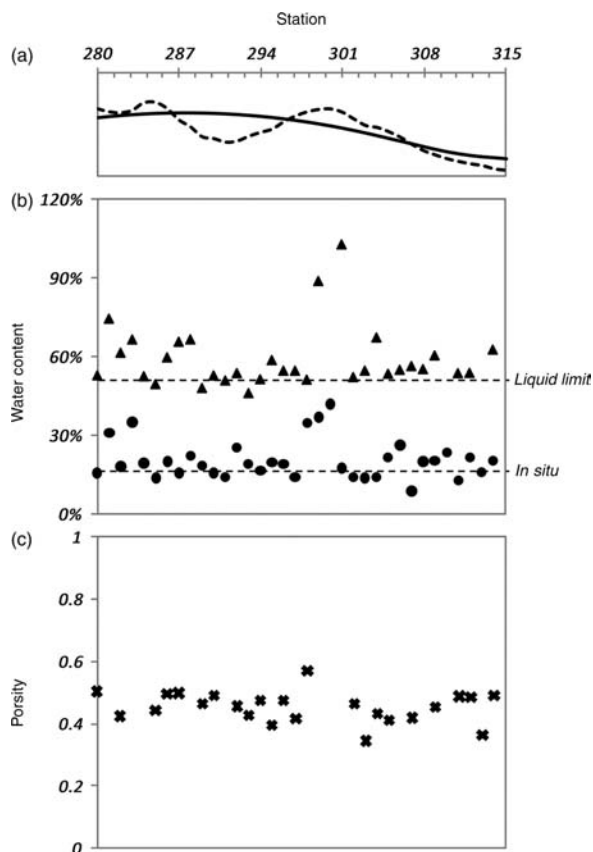

Figure 2.   Topography and subgrade. (a) Original topography (dashed line) and as-built longitudinal cross section showing cut and fill zones. The subgrade was characterised after compaction; samples recovered at every station were used to determine (b) liquid limit (filled triangles), *in situ* water content (filled circles) and (c) porosity.

requirements. Therefore, the upper 0.15 m of the subgrade had to be stabilised by mixing in crushed stone and re-compacting. Stabilisation work began on 23 July 2008 and was completed on 30 July 2008.

The construction of the cement-treated base took place between 30 July 2008 and 5 August 2008. Cement and aggregate were mixed in a pug mill and hauled for 3.2 km to the construction site. The mix contained 4% cement by weight and was compacted to 90% of the maximum dry density (modified Proctor). The mix was monitored from the time it left the pug mill until the final bituminous coat was applied to seal it. Spreading and compaction operations started at station $280 + 00$ and moved along the westbound lane towards station $314 + 00$. The eastbound lane was constructed on the way back, from station $314 + 00$ towards station $280 + 00$. Construction issues near the bridge approach (station $314 + 00$) led to a short gap in the test section near the bridge.

The placement and compaction of the unbound aggregate base started on 11 August 2008 and lasted for 18 days. The asphalt concrete layer was placed in two lifts. The first was a 19-mm NMS, 0.05-m thick layer built shortly after the completion of the unbound aggregate base on 16 October 2008. The riding surface was a 12.5 mm NMS, 0.04 m thick-layer added on 18 April 2009.

Laboratory and field material characterisation

The layers were carefully monitored during construction, including extensive material characterisation in the laboratory and in the field. Results are summarised in Table 1.

Subgrade

A total of 35 subgrade samples were collected from the test section and used to determine grain size distribution, specific surface, liquid limit, bulk density, water content, complex permittivity, electrical conductivity, suction and P-wave velocity in the laboratory. The field characterisation of the subgrade included dynamic cone penetrometer, helical probe test and surface waves. Test results are summarised in Table 1 and the main findings are as follows.

The mean grain size distribution is characterised by $D_{10} = 0.2$ mm, $D_{50} = 0.5$ mm, coefficient of uniformity $C_u = 6$ and coefficient of curvature $C_c = 1.3$, which are characteristics of well-graded granular materials. The fraction of fines ($d < 75\,\mu$m) ranged from 1% (at station $299 + 00$) to 36% (at station $306 + 00$). The fines exhibited high specific surface, suggesting the presence of clay minerals ($7-30\,\text{m}^2\,\text{g}^{-1}$), and susceptibility to changes in water content and/or pore fluid chemistry.

The recovered *in situ* water content data fall within the range of optimum water content established by the Proctor

Table 1. Laboratory and field material characterisation.

Layer (thickness)	Parameter	Measured value
Asphalt concrete (0.089 m)	Surface wave velocity, V_R (m s^{-1})	1000–2400
	P-wave velocity, V_p (m s^{-1})	3500–4100
Unbound aggregate base (0.158 m)	Surface wave velocity, V_R (m s^{-1})	200–300
Cement-treated base (0.254 m)	Electrical resistivity, $\rho_{electric}$ (Ω m)	800–5000
	P-wave velocity, V_p (m s^{-1})	2900–3400
	Surface wave velocity, V_R (m s^{-1})	1400–1900
	Compressive strength, σ (MPa)	3–5
Stabilised subgrade (0.158 mm)	Surface waves, V_R (m s^{-1})	200–300
Subgrade (< 12 m)	Coefficient of uniformity, C_u and curvature, C_c	6 and 1.3
	Fraction smaller than 75 μm	0.012–0.36
	D_{10} (mm)	0.09–0.25
	Specific surface, S_s (m^2 g^{-1})	7–30
	Liquid limit, LL (%)	50–100
	Water content, w (%)	15–40
	Penetration rate, PR (mm blow^{-1})	4–15
	Torque (HPT), T (N m)	5–12
	Porosity, n	0.3–0.5
	Matric suction, h_M (kPa)	50–500
	Osmotic suction, h_π (kPa)	100–1000
	P-wave velocity, V_p (m s^{-1})	300–800
	Surface waves, V_R (m s^{-1})	150–200

compaction tests carried out by GDOT. The measured liquid limit values are plotted in Figure 2(b) for reference. Total suction data gathered at the *in situ* water content fall between 200 and 1500 kPa. These suction levels anticipate a high moisture-dependent response of the subgrade.

The P-wave velocity in the unsaturated sediments is practically unaffected by the bulk stiffness of the fluid when the degree of saturation $S \leq 95\%$. Instead, it reflects the stiffness of the soil skeleton, which is in part controlled by the capillary forces, i.e. suction (Santamarina *et al.* 2001). P-wave velocities are measured in the laboratory using a pair of matching piezocrystals. The first transducer is connected to a wave generator and acts as a wave source, while the second transducer is located at the opposite end of the sample and acts as a wave receiver. The P-wave velocity is computed as the travel length divided by the travel time. The measured P-wave velocities for the subgrade are in the range from 300 to 800 m s^{-1}, in agreement with the high measured suction values, which suggest that capillarity controls the subgrade stiffness. It should be noted that only samples that satisfied the test geometric criterion where used to determine V_p. Since the soil samples that fulfilled this requirement were, for the most part, very well-compacted blocks, the measurement is biased to stiffer values and does not necessarily represent the average stiffness of the subgrade. The field-measured surface wave velocities range from $V_R = 150$ to 200 m s^{-1}.

The measured helical probe torque and dynamic cone penetration resistance are inversely correlated to both the total suction and the dry density; no evident correlation with bulk density or porosity was observed. Dynamic cone penetration data can be used in conjunction with density,

liquid limit and water content to estimate the resilient modulus of the subgrade (George and Uddin 2000):

$$E_R = a_o(PR)^{a_1}\left[\gamma_{dry}^{a_2} + \left(\frac{LL}{w_c}\right)^{a_3}\right] \qquad (1)$$

where PR is the dynamic cone penetration rate, γ_{dry} is the dry unit weight, LL is the liquid limit, w_c is the water content and a_i are fitting parameters. The estimated resilient modulus is $E_R = 250$ MPa, with a standard deviation of 100 MPa.

Cement-treated base

The off-site mixing, transport, spreading and compaction of the cement-treated base were carefully monitored to assess hydration prior to compaction. Electrical properties of curing cementitious materials vary as a function of hydration, pore fluid composition, moisture and temperature (Monfore 1968, Christensen *et al.* 1994, Fam and Santamarina 1996, McCarter 1996, McCarter *et al.* 1996, Revil and Glover 1997, Rajabipour and Weiss 2007). As the cement paste cures in a mortar mixture, there is a reduction in the ionic concentration of the pore fluid, which leads to measurable changes in electrical resistivity. Therefore, electrical resistivity data can be used to assess the curing evolution of the Portland cement mixtures. Curing of the compacted material was monitored using an electrical resistivity probe developed as part of this study. Different locations near the spreader were selected and tested in order to assess spatial variability and to detect heterogeneities. Results show no significant resistivity

differences from location to location, suggesting homogeneity in the construction process. After collection of the spatial variability data, the electrical resistivity monitoring equipment was fixed at a given location to monitor the time evolution of electrical resistance, which can be used as an index of the curing progress. Resistivity measurements started approximately 20–30 min after the cement was first exposed to water in the mixer. Field data show noticeable changes in conductivity starting at 100 min (Figure 3).

Characterisation of the hardened cement-treated base properties was done on 7-day cores recovered from the site and tested for laboratory P-wave velocity and compressive strength; a summary of results is presented in Table 1. A primary concern with the construction of the inverted pavement structure is the mechanical response of the cement-treated base during the compaction of the unbound aggregate layer above and its long-term integrity. Copper wire loops were installed within the cement-treated base surface at selected locations with the intent of monitoring changes in the loop resistance that could be associated with the development of fractures in the layer. A 6.35 mm-thick groove was cut 12.7 mm into the cement-treated base. Then, a thin polyurethane-coated copper wire, $d = 0.3$ mm, was placed in the grove and bonded to the sub-base using mortar mix. The resistance between the two ends was measured immediately after the installation of the wire to verify its integrity. The resistance at each of the three instrumented stations was measured following the construction of the unbound aggregate base; no changes from the pre-construction values were observed. These results indicate
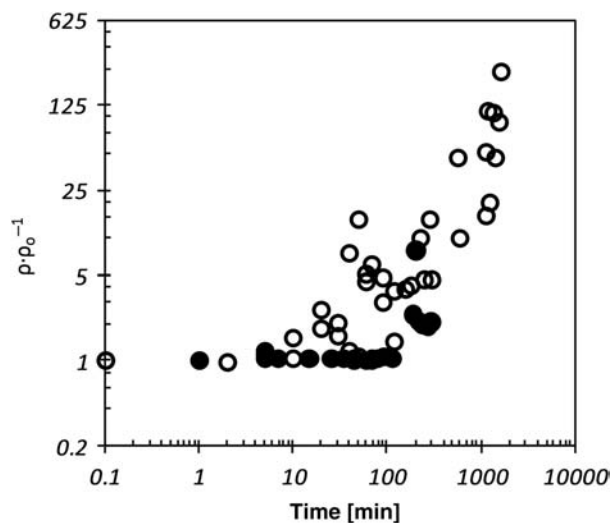

Figure 3.   Cement-treated base. Curing was monitored using a 4-electrode probe to determine electrical resistivity. Similar preliminary tests were conducted in the laboratory. Field data (filled circles) show an increase in resistivity starting at 100 min; laboratory specimens exhibit resistivity increases as early as 20 min after mixing (hollow circles).

that the cement-treated base sustained no significant damage during the compaction of the unbound aggregate and the asphalt concrete layers. Further confirmation of the layer integrity was accomplished through visual inspection during a forensic study. Note that while no indication of damage was observed, the number of tests is small and may not be representative of the entire length of the inverted pavement section.

Unbound aggregate base

The unbound aggregate base is the central component of the inverted pavement structure. Therefore, special attention was devoted to identify changes in the aggregate base properties caused by compaction over the stiff cement-treated base. Aggregate samples were recovered pre- and post compaction to determine grain size distribution in an effort to establish if crushing was taking place during compaction. Post-compaction samples were collected at three depths within the unbound aggregate base, i.e. top third, middle zone and bottom third. Grain size distribution data are summarised in Figure 4. Data from stations $290 + 00$ and $300 + 00$ indicate finer grain size distribution in the top third of the layer; furthermore, the fraction of material smaller than $75\,\mu$m is higher on all post-compaction samples than the pre-compaction gradation. While these results point towards some crushing, these limited results cannot be used to reach definitive conclusions as to the extent and significance of particle crushing on the densification of the unbound aggregate base.

The development of inherent anisotropy in the unbound aggregate layer as a result of compaction-induced particle alignment was assessed via a forensic study. Trenches were dug through the asphalt layer uncovering the unbound aggregate and allowing us to take a look inside the unbound aggregate base and photograph the grain skeleton. Digital image analysis results presented in Figure 5 show that particles preferentially align with their major axis parallel to the horizontal plane. Note that only particles coarser than 5 mm are considered in this analysis.

The as-built unloaded stiffness of the unbound aggregate base was determined using spectral analysis of surface waves (SASW) prior to the construction of the asphalt concrete layer. The unbound aggregate non-linear stiffness–stress response is critical to the mechanical response of an inverted pavement structure. The stiffness–stress relationship was determined using a novel laboratory procedure in which compressive wave propagation velocities in the vertical and radial directions are measured at various states of stresses. In the test, the unbound aggregate is mixed at the optimum water content, placed in a Proctor-type mold and compacted in a vibratory table for 15 min under a 240 N weight, i.e. a vertical stress of 13 kPa.
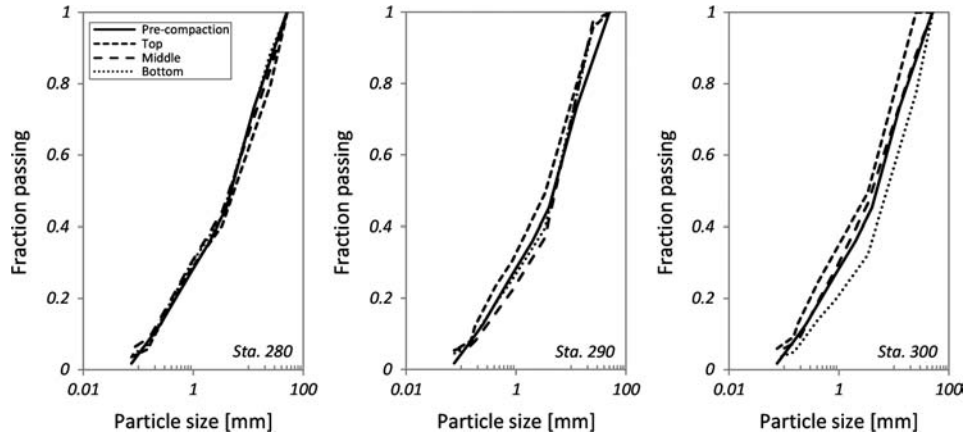
Figure 4. Pre- and post-compaction unbound aggregate base grain size distribution in the top, middle and bottom thirds for samples recovered at stations $280 + 00$, $290 + 00$ and $300 + 00$.

A dry density of $1925\,\text{kg}\,\text{m}^{-3}$ was achieved by this method, which corresponds to a 90% compaction (modified proctor). Two holes were then drilled through the compacted material to allow for the installation of piezoelectric sensors. The instrumented cell was placed in the loading frame and the sensors connected to the peripheral electronics. Signals were pre-amplified, filtered, digitised and stored into a laptop computer for processing and analysis.

The specimen undergoes 25 cycles of preconditioning loading and unloading, with vertical stress amplitude of $700\,\text{kPa}$. Unloading after the final cycle is stopped at a vertical stress of $14\,\text{kPa}$ to simulate the overburden. The first measurements are made starting at $14\,\text{kPa}$ and at every $80\,\text{kPa}$ until the vertical stress is $580\,\text{kPa}$, which is 83% of the maximum preconditioning vertical stress. The set of signals recorded at each load increment shows the strong stress dependency of the unbound aggregate (Figure 6(b)). These laboratory results and complementary field measurements allowed us to calibrate physically appropriate and simple stiffness–stress expressions of the following form (Van Niekerk *et al.* 2002):

$$E_{\text{R}} = k_1 \left(\frac{p}{p_0}\right)^{k_2} \left[1 - k_3 \left(\frac{q}{q_{\text{f}}}\right)^{k_4}\right], \tag{2}$$

where,

$$p = \frac{1}{3}\underline{\sigma} : \underline{1}, \quad q = \sqrt{\frac{3}{2}\underline{\sigma}' : \underline{\sigma}'\underline{1}} \quad \text{and} \quad \underline{\sigma}' = \underline{\sigma} - p\underline{1}$$

and p is the mean stress, q the deviatoric stress, q_f is the deviatoric stress at failure and k_i are material parameters. This non-linear elastic model consists of two stress terms and four fitting parameters. The p_{o} is a normalising stress, k_1 is the resilient modulus at $p = p_{\text{o}}$ and $q = 0$, $k_2 > 0$ captures the sensitivity of the resilient modulus to the mean stress, and $k_3 > 0$ and $k_4 > 0$ combine to capture skeletal softening induced by the deviatoric stress q in reference to the proximity to the failure load q_f. Guidance for the
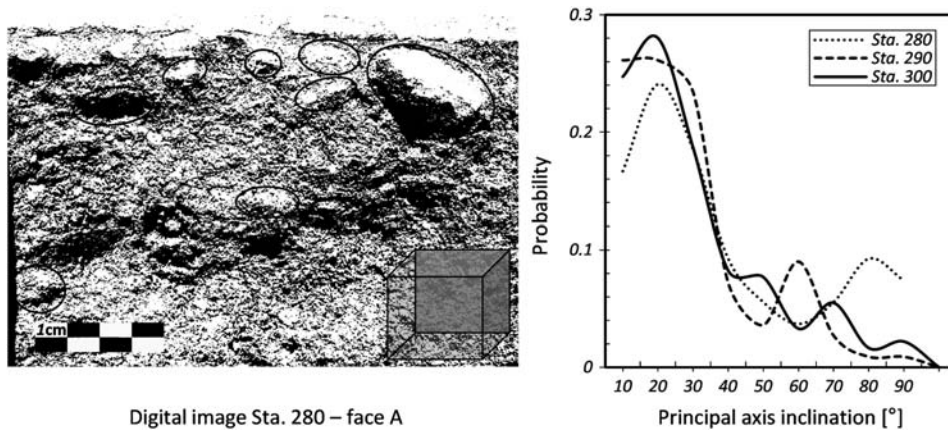

Figure 5. Preferential particle orientation from digital image processing of photographs taken during the forensic investigation. A typical image is shown on the left.
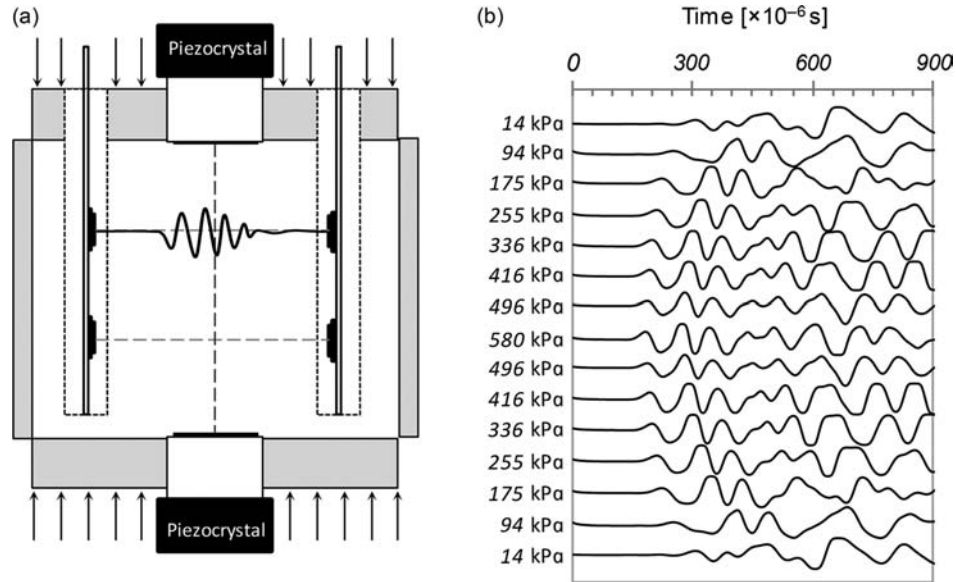
Figure 6. Unbound aggregate base: stress-dependent stiffness. (a) Instrumented laboratory zero lateral strain test cell. (b) Signature cascades as a function of the applied vertical stress clearly show shorter travel times at higher stress.

determination of physically meaningful k_2-values can be found in the elastic wave velocity literature (Kopperman *et al.* 1982, Hardin and Blandford 1989, Fam and Santamarina 1996). The values of k_2 can range from $k_2 = 0$ for cemented soils to $k_2 = 1.5$ in soils whose response is strongly influenced by electrical interactions. For unbound aggregates typically used in pavement bases and sub-bases, expected values can be found in the range from $k_2 = 0$ for cement-treated bases to 0.5 for rough/angular aggregates. The deviatoric stress-softening effect is controlled by k_3 and k_4. At $q = q_f$, the material reaches failure and the stress-softening term reduces to $1 - k_3$; thus, physically meaningful values of k_3 are in the range from $k_3 = 0$ (no-softening) to $k_3 = 1$ (flow at failure). The k_4 parameter captures the softening sensitivity of the material for a given deviatoric stress amplitude. Stiffness diminishes linearly with deviatoric loading if $k_4 = 1$. Typically, the effect of deviatoric loading is low when $q \ll q_f$ and increases as the material approaches failure, therefore $k_4 > 1$.

Asphalt concrete

The characterisation of the asphalt concrete layer focused on the determination of the elastic parameters, namely the elastic modulus and the Poisson's ratio. This was accomplished through field measurements of surface waves and laboratory P-wave velocity measurements in samples recovered during the forensic investigation.

The data were used to estimate the constrained modulus M using theory of elasticity and assuming isotropic stiffness. Using the *in situ* measured Rayleigh wave velocity data, V_R and the bulk density ρ:

$$M \approx 2\rho \left(\frac{V_R}{0.9}\right)^2 \frac{(1 - \nu)}{(1 - 2\nu)}. \qquad (3)$$

The values of constrained modulus along the test section are presented in Figure 7; the figure includes stiffness data for all the layers. The stiffness profile of the as-built pavement structure (without traffic load) ranges from 30,000 MPa for the asphalt concrete to 140 MPa for the subgrade.
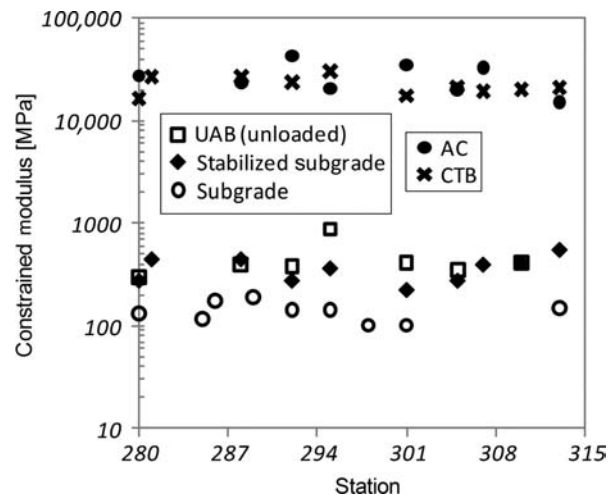

Figure 7. Asphalt concrete: stiffness. Wave propagation velocity was determined for each layer using high-resolution SASW. All measurements summarised in this figure show the high stiffness of the AC and CTB layers (low stress sensitivity) compared with the aggregate base and the subgrade (stress dependent – values shown are without load).

Table 2. Layers and material models used in the numerical simulation.

Asphalt concrete (t_{AC} = 0.089 m):
    Isotropic linear elastic
    E = 1.7 GPa
    ν = 0.35

Unbound aggregate base (t_{UAB} = 0.158 m):
    Isotropic non-linear elastoplastic

$$E_{Rz} = 200\,\text{MPa} \cdot \left(\frac{p}{1\,\text{kPa}}\right)^{0.2}\left[1 - 0.9 \cdot \left(\frac{q}{q_f}\right)^{16}\right]$$

$$E_{Rp} = 200\,\text{MPa} \cdot \left(\frac{p}{1\,\text{kPa}}\right)^{0.2}\left[1 - 0.9 \cdot \left(\frac{q}{q_f}\right)^{16}\right]$$

$$G^* = 76.9\,\text{MPa} \cdot \left(\frac{p}{1\,\text{kPa}}\right)^{0.2}\left[1 - 0.9 \cdot \left(\frac{q}{q_f}\right)^{16}\right]$$

    $\nu_{pp} = \nu_{zp} = 0.3$
    $\varphi = 40°$; C = 1 kPa

Cement-treated base (t_{CTB} = 0.254 m):
    Isotropic linear elastic
    E = 13.7 GPa
    ν = 0.2

Subgrade (t_{SG} = 2.54 m):
    Isotropic linear elastic
    E = 100 MPa
    ν = 0.2

Note: E, Young's modulus; ν, Poisson's ratio; E_{Rz}, Resilient modulus normal to the isotropic plane; E_{Rp}, Resilient modulus in the isotropic plane; G^*, shear modulus; ν_{pp}, Poisson's ratio in the isotropic plane; ν_{zp}, Poisson's ratio normal to the isotropic plane.

Preliminary analyses – numerical simulation

The inverted pavement system was modelled using the finite element software ABAQUS®. In these simulations, the asphalt concrete, AC and cement-treated base, CTB, were modelled as linear elastic media. The unbound aggregate base, UAB, and the subgrade, SG, were modelled as cross-isotropic, non-linear elastoplastic materials, in agreement with Equation (2). The stress-dependent stiffness is extracted from laboratory data, such as Figure 6(b), and complementary field data, which included surface wave velocity measurements conducted during construction. The constitutive model and model parameters used in the simulation are presented in Table 2. The algorithm was validated by comparison with the Boussinesq closed-form solution, standard ABAQUS® material models and published results obtained for multi-layered linear elastic pavement analysis software packages (details in Cortes *et al.* 2012). The tire–pavement system was modelled using a 3D axisymmetric mesh, with zero lateral displacement boundaries at the edge of the pavement, zero vertical displacement at the foundation of the structure and no-slip between the layers. CAX8R, axisymmetric, eight-node elements and a two-by-two integration point scheme were used in the simulation. The load on the pavement was modelled using a 550 kPa tire contact pressure over a circular area of radius, r = 0.15 m.

The resulting vertical, radial and shear stress distributions along the centerline beneath the wheel are presented in Figure 8(a). Vertical stresses along the centerline are compressive throughout the full depth of influence of the load, and become negligible within the cement-treated base; by equilibrium, the vertical stress is the same above and below all interfaces. Radial stresses range from compression at the top to tension at the bottom of the asphalt concrete layer and cement-treated base; however, the radial stress is in compression in the unbound aggregate base and in the subgrade, in agreement with the Mohr–Coulomb strength criterion, so that the stress ratio remains $\sigma_z/\sigma_r \leq \tan^2(45 + \phi/2)$ throughout these layers. Radial slices of the vertical stress field are shown at interfaces in Figure 8(b). The vertical stress caused by the wheel load diminishes with depth; the peak vertical stress on the subgrade is less than 5% of the vertical stress applied on the surface.
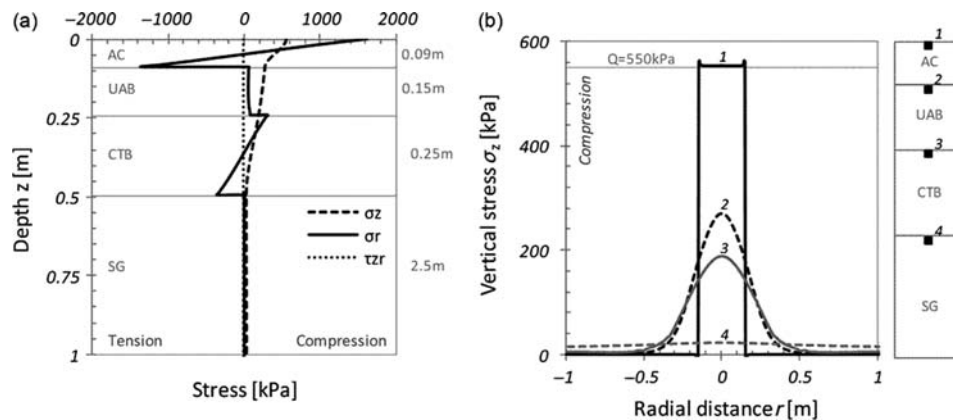

Figure 8. Induced stresses in an inverted pavement beneath a wheel modelled as a 550 kPa uniformly distributed load over a circular area of radius 0.15 m. (a) Vertical σ_z, radial σ_r and shear τ_{zr} stress profiles as a function of depth along the load centerline. (b) Radial profiles of induced vertical stresses at multiple locations within the inverted pavement structure.

Conclusions

The full-scale test section in LaGrange, GA, USA, offered a unique opportunity to characterise with unprecedented detail the properties of the different layers during construction of an inverted pavement structure. This information is of critical importance for the understanding of these pavement structures and to support numerical models and simulations.

The as-built inverted pavement structure stiffness profile exhibits pronounced contrast among successive layers; 30,000 MPa at the asphalt concrete, 500 MPa for the unbound aggregate base (unloaded), 22,000 MPa for the cement-treated base and 150 MPa for the compacted subgrade. This unconventional high-low-high-low stiffness sequence is a salient characteristic of inverted pavement systems.

The average measured specific surface and coefficient of uniformity of the subgrade at LaGrange indicate that its mechanical behaviour is strongly influenced by electrical interactions and capillarity; therefore, the mechanical response of the subgrade is susceptible to changes in water content and pore fluid chemistry. The high P-wave velocity values, measured as part of this study, reflect the importance of suction.

The off-site mixing, followed by transport, spreading and compaction of the cement-treated base resulted in a homogeneous layer. No early setting of the cement mixture was observed. The 7-day cured cement-treated base withstood the heavy compaction equipment used to attain high density in the overlaying unbound aggregate layer. Results from the integrity tests show no evidence of cracking.

The unbound aggregate base stiffness is a non-linear function of the state of stresses. The stiffness–stress relationship can be adequately determined in instrumented zero lateral strain cells. Pre- and post-compaction gradation test results do not offer a clear assessment of the extent and significance of particle crushing in the unbound aggregate layer during compaction over the stiff cement-treated base. Digital image analysis confirmed particle alignment inducing inherent anisotropy in the as-built unbound aggregate base.

Preliminary numerical results obtained with proper material models for the unbound aggregate layers confirm acceptable stresses in the various layers under the design traffic loads.

Acknowledgements

References

Ahlvin, R.G., *et al.*, 1971. *Multiple-wheel heavy gear load pavement tests*. Vicksburg: Army Corps of Engineers.

Barker, W.R., Brabston, W.N., and Townsend, F.C., 1973. *An investigation of the structural properties of stabilized layers in flexible pavement systems*. Vicksburg: U.S. Army Corps of Engineers.

Barksdale, R.D., 1984. Performance of crushed-stone base courses. *Transportation Research Record*, 954, 78–87.

Beatty, T.L., *et al.*, 2002. *Pavement preservation technology in France, South Africa, and Australia*. Alexandria, VA: Office of International Programs, Federal Highway Administration, U.S. Department of Transportation, and the American Association of State Highway and Transportation Officials.

Christensen, B.J., *et al.*, 1994. Impedance spectroscopy of hydrating cement-eased materials – measurement, interpretation, and application. *Journal of the American Ceramic Society*, 77 (10), 2789–2804.

Cortes, D.D., 2010. Inverted base pavement structures. Thesis (PhD). Atlanta, GA: Georgia Institute of Technology.

Cortes, D.D., Shin, H., and Santamarina, J.C., 2012. Numerical simulation of inverted pavement systems. *Journal of Transportation Engineering*, in press.

Fam, M.A. and Santamarina, J.C., 1996. Study of clay–cement slurries with mechanical and electromagnetic waves. *Journal of Geotechnical Engineering*, 122 (5), 365–373.

George, K.P. and Uddin, W., 2000. *Subgrade characterization for highway pavement design*. Jackson: Mississippi Department of Transportation Research Division.

Grau, R.W., 1973. *Evaluation of structural layers in flexible pavement*. Vicksburg: U.S. Army Corps of Engineers.

Hardin, B.O. and Blandford, G.E., 1989. Elasticity of particulate materials. *Journal of Geotechnical Engineering*, 115 (6), 788–805.

Horne, D., *et al.*, 1997. *South African pavement and other highway technologies and practices*. Federal Highway Administration U.S. Department of Transportation.

Jooste, F.J. and Sampson, L., 2005. *The economic benefits of HVS development work on G1 base pavement*. Lynn East, Department of Public Transport, Roads and Works Gauteng Provincial Government.

Kopperman, S.E., Stokoe, K.H., and Knox, D.P., 1982. *Effect of state of stress on velocity of low amplitude compression waves propagating along principal stress directions in dry sand*. Austin: University of Texas.

McCarter, W.J., 1996. Monitoring the influence of water and ionic ingress on cover-zone concrete subjected to repeated absorption. *Cement Concrete and Aggregates*, 18 (1), 55–63.

McCarter, W.J., Ezirim, H., and Emerson, M., 1996. Properties of concrete in the cover zone: water penetration, sorptivity and ionic ingress. *Magazine of Concrete Research*, 48 (176), 149–156.

Monfore, G.E., 1968. Electrical resistivity of concrete. *Journal of the PCA Research and Development Laboratories*, 10 (2), 35–48.

Rajabipour, F. and Weiss, J., 2007. Electrical conductivity of drying cement paste. *Materials and Structures*, 40 (10), 1143–1160.

Rasoulian, M., Becnel, B., and Keel, G., 2000. Stone interlayer pavement design. *Transportation Research Record*, 1709, 60–68.

Rasoulian, M., *et al.*, 2001. *Long term performance of stone interlayer pavement*. Baton Rouge: Louisiana Transportation Research Center.

Revil, A. and Glover, P.W.J., 1997. Theory of ionic-surface electrical conduction in porous media. *Physical Review B*, 55 (3), 1757–1773.

Rust, F.C., Mahoney, J.P., and Sorenson, J.B., 1998. *An international view of pavement engineering*. Trondheim: Bearing Capacity of Roads and Airfields.

Santamarina, J.C., Klein, K.A., and Fam, M.A., 2001. *Soils and waves*. New York: John Wiley & Sons, Ltd.

Tutumluer, E. and Barksdale, R.D., 1995. Inverted flexible pavement response and performance. *Transportation Research Record*, 1482, 102–110.

Van Niekerk, A.A., Molenaar, A.A.A., and Houben, L.J.M., 2002. Effect of material quality and compaction on the mechanical behaviour of base course materials and pavement performance. *6th international conference on bearing capacity of roads, railways and airfields*, Lisbon, Portugal.